

Continuous glacier mass changes in High Mountain Asia based on ICESat-1,2 and GRACE/GRACE Follow-on data

Qiuyu Wang¹, Shuang Yi², and Wenke Sun³

¹University of Chinese Academy of Sciences

²University of Stuttgart

³Key Laboratory of Computational Geodynamics, Chinese Academy of Sciences

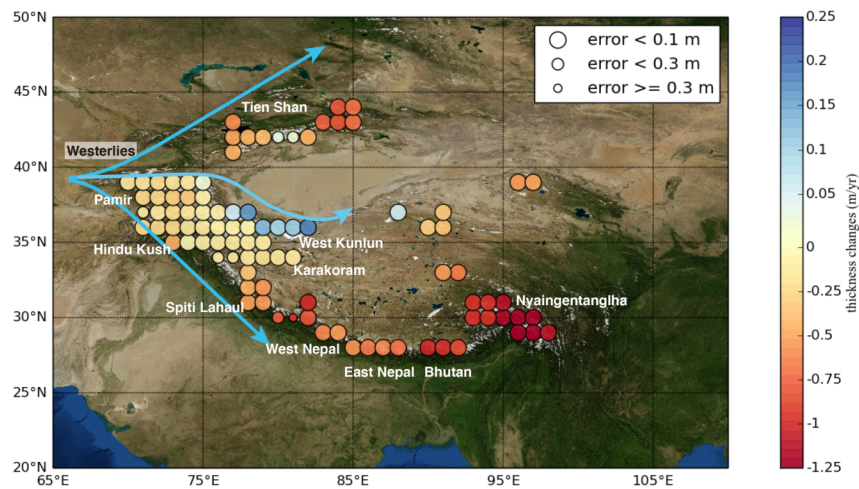
November 21, 2022

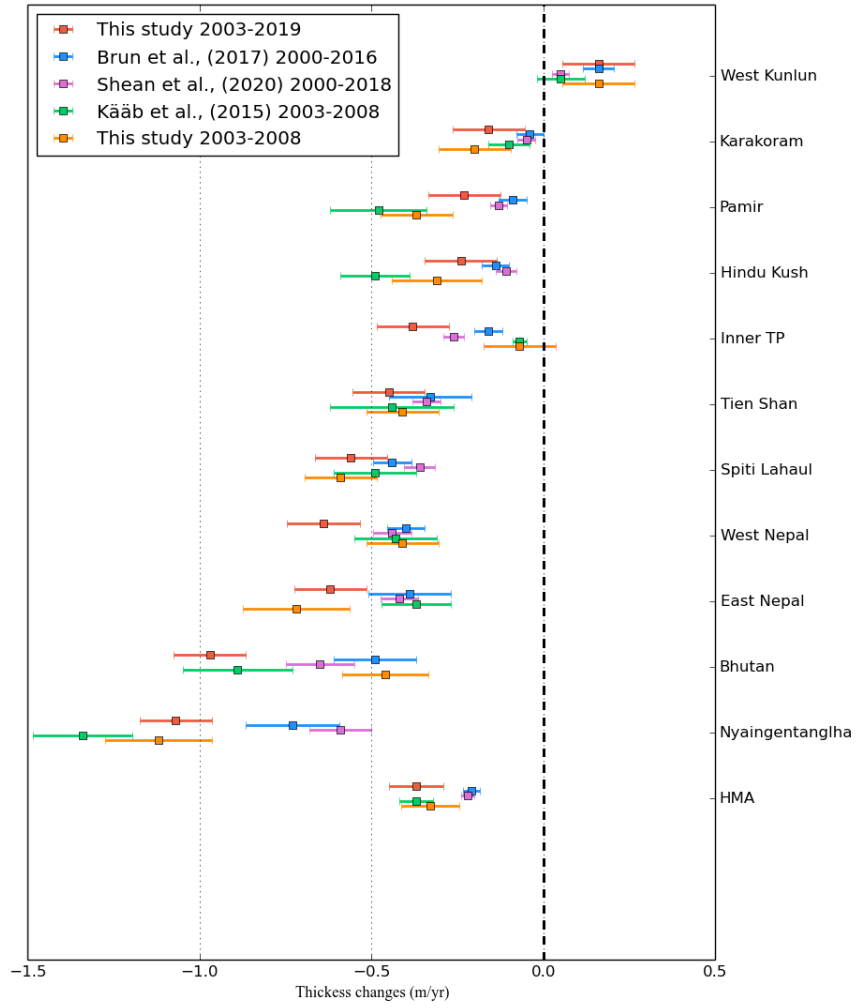
Abstract

Glacier melt in High Mountain Asia (HMA) is an indicator of climate change, and has a major impact on the regional hydrology and freshwater supply. We determined the recent states of the HMA glaciers based on the first analysis of Ice, Cloud, and Land Elevation Satellite-2 (ICESat-2) data. We used the Gravity Recovery and Climate Experiment (GRACE) and GRACE-FO data to fill the gap of ICESat-1,2 and carry out an independent validation. The agreement between ICESat-1,2 and GRACE/GRACE-FO data at the total and regional scales demonstrates the high reliability of results. Based on ICESat-1,2, the total mass change of the HMA glaciers is -28 ± 6 Gt yr⁻¹ from 2003-2019, which are more negative than stereo imagery based literature. The spatial variability of the glacier indicates rapid thinning in Nyaingentanglha but a slight increase in West Kunlun. ICESat-2 enable new insight into the continuous measurement of the HMA glacier.

Hosted file

p5sp_submit.docx available at <https://authorea.com/users/528428/articles/596868-continuous-glacier-mass-changes-in-high-mountain-asia-based-on-icesat-1-2-and-grace-grace-follow-on-data>





1 **Continuous glacier mass changes in High Mountain Asia based on ICESat-1,2**
2 **and GRACE/GRACE Follow-on data**

3 Qiuyu Wang¹, Shuang Yi², Wenke Sun^{1,*}

4 ¹Key Laboratory of Computational Geodynamics, University of Chinese Academy of
5 Sciences, Beijing 100049, China.

6 ²Institute of Geodesy, University of Stuttgart, Stuttgart, Germany

7 *Corresponding author: E-mail: sunw@ucas.ac.cn

8

9

10

11 Key points:

12 1. We provide the first look of ICESat-2 data on glacier thickness and mass changes
13 in the High Mountain Asia.

14 2. We use independent data from satellite gravimetry to fill data gap of ICESat, and
15 obtain nearly continuous glacier mass changes.

16 3. There is a quantitative agreement in between satellite gravimetry and satellite
17 altimetry, which show high reliability of result and data

18

19 Abstract:

20

21 Glacier melt in High Mountain Asia (HMA) is an indicator of climate change, and has
22 a major impact on the regional hydrology and freshwater supply. We determined the
23 recent states of the HMA glaciers based on the first analysis of Ice, Cloud, and Land
24 Elevation Satellite-2 (ICESat-2) data. We used the Gravity Recovery and Climate
25 Experiment (GRACE) and GRACE-FO data to fill the gap of ICESat-1,2 and carry
26 out an independent validation. The agreement between ICESat-1,2 and
27 GRACE/GRACE-FO data at the total and regional scales demonstrates the high
28 reliability of results. Based on ICESat-1,2, the total mass change of the HMA glaciers
29 is -28 ± 6 Gt yr⁻¹ from 2003–2019, which are more negative than stereo imagery
30 based literature. The spatial variability of the glacier indicates rapid thinning in
31 Nyaingentanglha but a slight increase in West Kunlun. ICESat-2 enable new insight
32 into the continuous measurement of the HMA glacier.

33

34 Plain abstract:

35

36 High Mountain Asia is the largest ice-covered region outside the polar regions.
37 Glaciers have been melting for the past decades due to global warming and the
38 melting will probably continue in the coming decades. This will threaten the water
39 availability in downstream basins and affect the regional or global climate. Thus, it is
40 important to continuously monitor the states of the glaciers. In this study, the first
41 analysis of data released after the launch of the second generation of the Ice, Cloud,
42 and Land Elevation Satellite (ICESat-2) is provided. The data were used to survey the
43 glacier thickness and mass change in High Mountain Asia. We used independent
44 gravity satellite data to fill the gap of ICESat, The two independent datasets agree
45 with respect to the continuous glacier mass change, which indicates the high
46 reliability of the results. Based on our results, the continuous glacier mass change
47 from 2003–2019 is on average -28 ± 6 Gt yr⁻¹ (Gt = 10⁹ t water) or -0.34 ± 0.07 m yr⁻¹
48 (thickness change). The regional variability of the glaciers ranges from -1.07 ± 0.10 m
49 yr⁻¹ in southeastern Nyaingentanglha to $+0.16 \pm 0.10$ m yr⁻¹ in West Kunlun.

50

51 1. Introduction

52 High Mountain Asia (HMA) contains the largest ice-covered region outside the
53 south and north poles (Qiu, 2008). Meltwater from glaciers and snow, the head of
54 several large rivers, is a major source of drinking water and irrigation for several
55 hundred million people (Immerzeel and Bierkens, 2012). Recent reports revealed that
56 these glaciers have been dwindling for the past several decades (Bolch *et al.*, 2012;
57 Yao *et al.*, 2012; Azam *et al.*, 2018; Yao *et al.*, 2019). Future projections indicate that
58 glacier shrinkage due to global warming will continue in the coming decades, which
59 will aggravate the regional water scarcity, especially in subhumid to arid climates,
60 thus affecting economic activities and the political stability (Pritchard, 2019).
61 Strategies for the continuous monitoring the states of glaciers are therefore critical for
62 climate change studies and the local management of water resources (Immerzeel *et al.*,
63 2020). Compared with the interpolation of *in situ* measurements and physical glacier
64 change models, satellite observations are more effective in surveying large-scale
65 glaciers in remote areas crossing political boundaries. The results of numerous studies
66 indicated the practical application of satellite data. Satellite strategies can be divided
67 into two categories:

68 1) Measurement of geometry including surface height and area. Satellites
69 detecting height changes include laser altimetry (i.e., Ice, Cloud, and Land Elevation
70 Satellite ICESat (Neckel *et al.*, 2014; Wang *et al.*, 2017a; Treichler *et al.*, 2019) and
71 satellite stereo imagery (i.e., SPOT and ASTER; (Gardelle *et al.*, 2012; Gardelle *et al.*,
72 2013).

73 2) Measurement of the Earth's gravity field. Satellite gravimetry data from the
74 Gravity Recovery and Climate Experiment (GRACE) were used to calculate the mass
75 change (Velicogna, 2009; Matsuo and Heki, 2010; Jacob *et al.*, 2012; Yi *et al.*, 2016).

76 For the first time since the terrain correction method has been proposed for
77 ICESat data processing ICESat data analysis, the thickness changes in the Himalaya
78 and surrounding regions were analyzed (Kääb *et al.*, 2012). Subsequent ICESat-based
79 research considered additional areas and clustering algorithms. The glacier mass loss
80 from 2003–2008/2009 was estimated to be -20 to -24 Gt/yr in the Tibetan Plateau and
81 -24 to -29 Gt yr⁻¹ in the HMA (Tibetan Plateau and Tien Shan; (Gardner *et al.*, 2013;
82 Treichler *et al.*, 2015; Wang *et al.*, 2018). The short operational period of ICESat-1
83 and sparse spatial sampling led to potential large bias. Since the launch of ICESat-2 in
84 2018, the temporal coverage has been significantly expanded.

85 In satellite stereo imagery-based studies, the difference between Digital
86 Elevation Models (DEM) is calculated or linear regression is applied to time series of
87 DEM pixels derived from stereo imagery (Brun *et al.*, 2017; Shean *et al.*, 2020).
88 Compared with ICESat, stereo imagery-based studies have a higher spatial coverage
89 and longer time span. Earlier stereo imagery-based studies only covered glaciers in
90 parts of the HMA (Gardelle *et al.*, 2012; Gardelle *et al.*, 2013). Burn *et al.* (2017)
91 recently calculated a mass change of 92% at a rate of -16 ± 4 Gt yr⁻¹ for the glacier
92 area in the HMA from 2000 to 2016. Shen *et al.* (2020) used stereo imagery data and

93 estimated that the HMA glacier mass has changed by approximately $-19 \pm 3 \text{ Gt yr}^{-1}$
94 from 2000–2018. Note that these mass budgets are less negative than those of most
95 previous studies. Limited by the number of available DEMs, satellite stereo imagery
96 has a low temporal resolution. Few time series of glacier mass/thickness changes are
97 based on satellite stereo imagery, which makes it difficult to continuously monitor
98 recent glacier states and the strong temporal variability.

99 Satellite gravimetry data from GRACE provides monthly Earth gravity fields,
100 demonstrating the feasibility of the use of GRACE data for the monitoring of glaciers,
101 ice caps, water storage in global basins, and sea level changes. The difficulty of the
102 application of GRACE in HMA is mainly due to the strong influence of terrestrial
103 water storage such as increasing water storage of lakes in the Inner Tibetan Plateau
104 (ITP). Early GRACE-based studies reported a glacier mass loss ranging from -47 to
105 -4 Gt/yr from 2003 to 2009/2010 due to the misinterpretation of other hydrological
106 mass changes (*Matsuo and Heki, 2010; Jacob et al., 2012*). Based on more
107 contributions and cautious verifications by scholars, the updated mass budget of
108 HMA glaciers varied from -29 to -19 Gt yr^{-1} in the period 2003–2009 (*Gardner et al.,*
109 *2013*), from -35 to -17 Gt yr^{-1} during 2003–2013 (*Schrama et al., 2014; Yi and Sun,*
110 *2014*), and from -24 to -18 Gt yr^{-1} in the period of 2003–2015/2016 (*Wang et al.,*
111 *2018; Wouters et al., 2019*).

112 These studies were mostly carried out in variable, short time periods, which
113 makes it difficult to compare the estimates and establish a consensus. Compared with
114 glacier mass budgets, the time series of glaciers include detailed information on the
115 glacier evolution and can be used to quantify the acceleration or deterioration of
116 recent glacier changes. Similarly, the time series of glaciers provide more constraints
117 for the calibration of the prediction models that are used for the projection of the
118 relationship between glaciers and climate change. In a more recent study using
119 GRACE and GRACE Follow-on (FO) data, the HMA glacier loss was estimated at a
120 rate of $-29 \pm 12 \text{ Gt/yr}$ over a longer period from 2002 to 2019 (*Ciraci et al., 2020*). To
121 confirm the reliability of GRACE/GRACE-FO and fill the data gap, the authors
122 determined the glacier surface mass balance using independent data from the NASA
123 Modern-Era Retrospective Analysis for Research and Application (MERRA-2)
124 reanalysis. The MERRA-2 is the latest atmospheric reanalysis result and is in
125 excellent agreement with GRACE/GRACE-FO at the regional scale of global glaciers
126 and ice caps, except for the HMA glacier. The corrected terms such as GIA, LIA in
127 *Ciraci et al. (2020)* account for ~60% of the total mass budget of the HMA glaciers.
128 However, the accuracy of these corrections is difficult to assess. It may be cautious
129 when using the corrected terms. Therefore, further studies are required to estimate the
130 mass loss of the HMA glaciers.

131 In this study, ICESat-1 and 2 data were used for the first time to construct the
132 glacier surface elevation in the HMA for the periods 2003–2009 and 2018–2019. The
133 data were combined with GRACE and GRACE-FO to fill data gaps. Our aim was to
134 establish a consensus based on long time series of glacier mass/thickness changes

135 (2003–2019) in the whole HMA area and its four subdivisions. We determined the
136 change in the HMA glacier thickness during the period 2003–2019 based on two
137 generations of altimetry satellites, that is, ICESat-1,2. More recent glaciers were
138 analyzed using two dependent satellites.

139

140 **2. Data and method**

141 2.1 ICESat-1 and ICESat-2 data

142 The ICESat-2 is the second generation of the laser altimeter ICESat mission,
143 which was launched in 2018 to measure the ice sheet mass change, cloud and aerosol
144 heights, land topography, and vegetation characteristics (*Markus et al.*, 2017). Similar
145 to the first ICESat mission (ICESat-1), ICESat-2 also is also equipped with a laser
146 altimeter, that is, the Advanced Topographic Laser Altimetry System (ATLAS),
147 which utilizes laser pulses that bounce off the Earth's surface, return to the satellite,
148 and record the traffic time pulses. To more accurately measure the Earth's surface
149 height, the ICESat-2 laser is split into six beams. Compared with the laser on
150 ICESat-1, which sends 40 pulses per second, ICESat-2's laser is fast-firing and sends
151 10,000 pulses per second (Neumann et al., 2018, 2019). Thus, ICESat-2 has a denser
152 footprint than ICESat-1.

153 Our analysis of the changes in the thickness of the HMA glacier is based on the
154 ICESat-2 L3A Land Ice Height (ATL06). This dataset includes geolocated land-ice
155 surface heights (above the WGS 84 ellipsoid) and ancillary parameters, which are
156 used to interpret and assess the quality of the surface heights (*Smith et al.*, 2020).
157 Over the ice sheet interior, the accuracy of ATL06 is better than 3 cm and the
158 precision of surface measurements is better than 9 cm (*Brunt et al.*, 2019). Similarly,
159 ICESat-1 data were used for the period 2003–2009 in this study. We used the Global
160 Land Surface Altimetry Data (GLA14) of ICESat-1.

161 The preprocessing was described in Wang et al. (2017b) and is similar to that
162 reported in other studies (*Gardner et al.*, 2013; *Farinotti et al.*, 2015): extraction of
163 the footprint, height conversion, determination of the elevation difference (ICESat
164 and Shuttle Radar Topography Mission, SRTM), and removal of outliers. The
165 calculation of the average change in the glacier thickness is based on the elevation bin
166 method (*Wang et al.*, 2017b). The idea of this method is that 1) the elevation
167 differences between ICESat footprints and SRTM are defined as dh (one valid ICESat
168 footprint corresponding to one dh value); 2) glaciers are divided into numerous
169 elevation bins according to their altitude distribution; 3) the elevation difference of
170 each bin (defined as Dh) equals the median of all footprints' dh values in this bin (one
171 elevation bin corresponding to one Dh); and 4) the elevation difference of the entire
172 glacier (defined as DH) is the area-weighted Dh of all bins. We repeated the
173 calculation for different bin widths ranging from 100 to 600 m spaced at 100 m
174 intervals. The final result is the average bin width. The DH change is a time series of
175 the glacier thickness. Glacier thickness changes are converted to mass changes using a

176 density of 850 kg m^{-3} (Huss, 2013) which is appropriate for a wide range of
177 conditions.

178

179 2.2 GRACE and GRACE-FO data

180 In this study, the latest releases of the monthly GRACE and GRACE-FO
181 Release-6 (RL06) Stokes coefficients from 2003 to 2020 from the Center for Space
182 Research at the University of Texas (CSR) were used (Bettadpur, 2012). The
183 low-degree term of GRACE was processed for consistency with all other GRACE
184 solutions used in the science community. The degree 1 terms are based on a
185 combination of GRACE and ocean model outputs (Swenson *et al.*, 2008). The degree
186 2 order 0 spherical harmonic coefficient uses satellite laser ranging to replace the
187 GRACE coefficient (Cheng *et al.*, 2013).

188 The glacier mass change time series were calculated using the least-squares
189 mascon approach of Yi and Sun. (2014). Each mascon is an arbitrarily defined area
190 consisting of $0.5^\circ \times 0.5^\circ$ latitude cells. The distribution of the mascons was optimized
191 to follow the distribution of the glacier. We also placed mascons in the surrounding
192 region to alleviate or separate the leakage of other mass sources. The total water
193 storage estimated by GRACE is composed of the soil moisture storage, groundwater
194 storage, glacial isostatic adjustment (GIA), and unknown sources. In this study, land
195 water and GIA models were used to estimate the soil moisture storage and GIA
196 components, respectively.

197

198 2.3 Ancillary data

199 1) DEM data

200 Because of large cross-track gaps and rough terrain in the HMA region, a
201 full-area DEM reference can be used to correct topographic differences in ICESat
202 sampling footprints (Kääb *et al.*, 2012). In this study, the DEM from the SRTM (Farr
203 *et al.*, 2007) 1 Arc-Second Global elevation data provided was used, similar to
204 previous research.

205 2) Glacier boundary data

206 To distinguish glaciers from land, the latest version of the Randolph Glacier
207 Inventory 6.0 (RGI6.0) was used in this study (Pfeffer *et al.*, 2014), which is based on
208 a Global Land Ice Measurements from Space (GLIMS) project (RGI Consortium
209 2017).

210 3) Soil water model

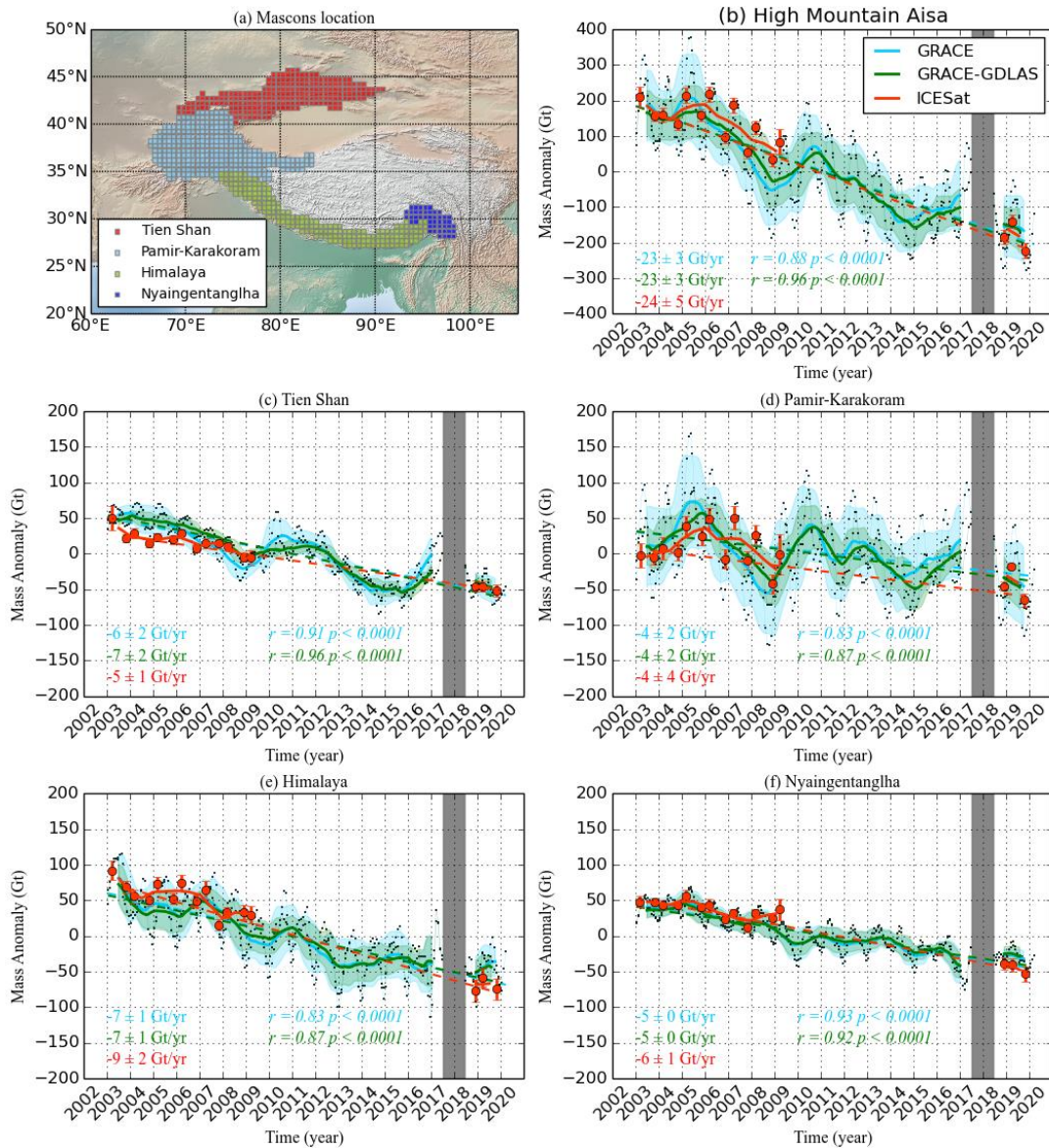
211 Because of the leakage of other hydrological signals, the soil water model was
212 provided by the Global Land Data Assimilation System (GLDAS) to separate the soil
213 water components from the total mass. The soil water storage model extends to a
214 depth of several meters at a high resolution and in near real time. The GLDAS-2.1
215 model was used in this study (Rodell and Beaudoing, 2016).

216 4) GIA model

217 A GIA model was applied based on the model ICE6G to separate the GIA effect
 218 (*Argus et al., 2014; Peltier et al., 2015*). This model was used to calculate geodetic
 219 and geologic signals of the Earth such as the rate of radial displacement.
 220

221 3. Results

222 The gravity signal of GRACE in the ITP is dominated by increasing masses of
 223 lakes, groundwater, and soil water (*Zhang et al., 2013; Wang et al., 2016*), which is
 224 contrary to the glacier change based on field observations (*Yao et al., 2012*).
 225 Therefore, in this study, glaciers in the ITP are excluded from the GRACE-based
 226 estimate of the HMA glacier mass change. Most HMA glaciers are distributed on the
 227 periphery of the Tibetan Plateau, accounting for 85% of the total HMA glacier area.
 228 These peripheral glaciers can be divided into four subregions. Mascons were placed in
 229 these areas (Fig. 1a).



231 Figure 1. Mascon partitions for the HMA glacier (a) and time series of glacier mass
232 changes in four subregions (c, d, e, f) and their sum (b). A one-year average sliding
233 window is applied to GRACE (solid blue line), GRACE-GLDAS (solid green line),
234 and ICESat-derived glacier mass (solid red line). The colored value is the changing
235 rate based on the linear regression model. The color corresponds to the line color. The
236 r value is Pearson's correlation coefficient between ICESat and GRACE(blue
237 r)/GRACE-GLDAS(green r). The parameter $1-p$ presents the provability of the pass
238 correlation test.

239 3.1 Continuous time series of the glacier mass change

240 We constructed time series of the glacier mass change based on GRACE and
241 ICESat for the four subregions (Figs 1c–f). Their sum is shown in Fig. 1b. A one-year
242 average sliding window was applied to improve the signal-to-noise ratio, similar to
243 most GRACE-based studies. We removed the soil moisture based on the GLDAS
244 model (Fig. 1, green line) to isolate the glacier signals. The correlation coefficients
245 were calculated to quantify the consistency between ICESat and GRACE-derived
246 glacier mass changes. Based on the comparison of the results, three key points can be
247 discussed.

- 249 1. The data gap between ICESat-1 and 2 was filled with GRACE data,
250 although GRACE data also have a one-year data gap. The ICESat-based
251 glacier mass changes agree with those of GRACE with respect to the
252 changing trends and interannual fluctuations. The agreement is better in the
253 whole HMA area (except for ITP) than in the subregions.
- 254 2. After removing the soil moisture from GRACE-based mass changes (i.e.,
255 GRACE-GDLAS), the agreement with the ICESat result significantly
256 increased. The GRACE-based mass change includes ample surface snow or
257 land water caused by short-term precipitation. The GDLAS model contains
258 the part mass; thus, the GRACE-GDLAS result is more consistent with the
259 ICESat observation than the GRACE result alone.
- 260 3. The GLDAS-based soil moisture does not show a significant trend; thus, the
261 mass change trends of GRACE-GLDAS and GRACE are similar. This
262 might be reasonable. The soil moisture might only fluctuate seasonally and
263 show no trend over a long period.

264 3.2 Total glacier mass budget

265 We only used ICESat data and calculated the ITP glacier change to be
266 approximately $-4 \pm 2 \text{ Gt yr}^{-1}$ (Fig. S1). The total mass change of the HMA glacier is
267 $-28 \pm 6 \text{ Gt yr}^{-1}$ ($-0.29 \pm 0.06 \text{ m w.e. yr}^{-1}$, $-0.34 \pm 0.07 \text{ m yr}^{-1}$) based on ICESat-1,2
268 from March 2003 to November 2019. The glacier mass loss in the HMA from 2003–
269 2019/2020 excluding the ITP region is $-24 \pm 6 \text{ Gt yr}^{-1}$ based on ICESat and $-23 \pm 3 \text{ Gt}$
270 yr^{-1} based on GRACE. After removing the GIA effect, the GRACE-based mass
271 budget of the glacier becomes $-28 \pm 3 \text{ Gt yr}^{-1}$.

273

274

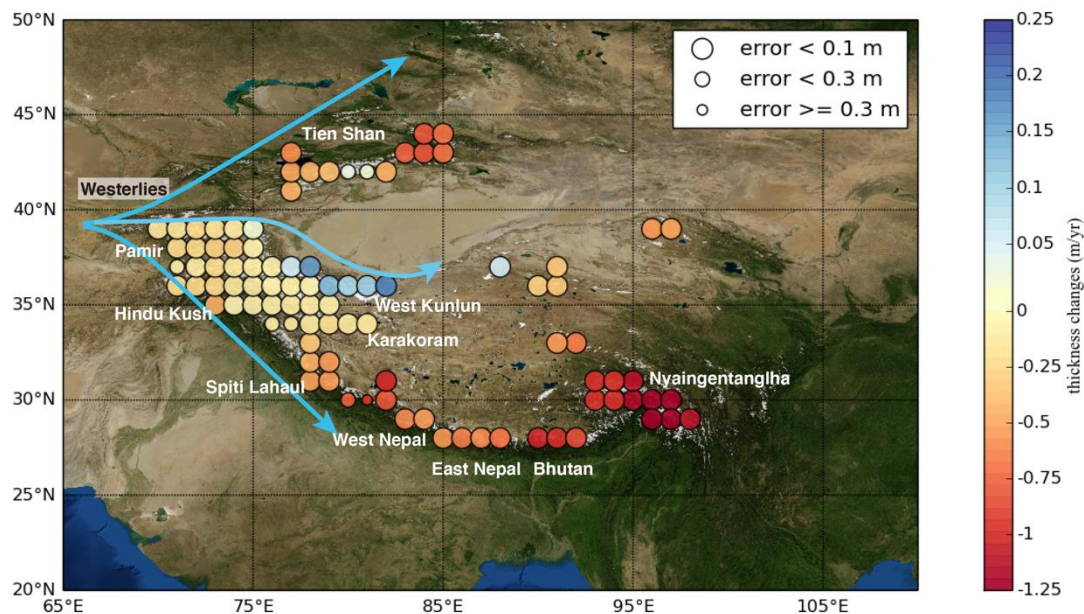
3.3 Spatial variability of the change in the glacier thickness

275

276

We present the detailed spatial distribution of the change in the glacier thickness in a $1^\circ \times 1^\circ$ grid based on ICESat-1,2 (Fig. 2). From 2003–2019, the change trend of regional glaciers varied from $-1.07 \pm 0.10 \text{ m yr}^{-1}$ in Nyaingentanglha to $+0.14 \pm 0.10 \text{ m yr}^{-1}$ in West Kunlun, indicating a large regional variability of the glacier change. The HMA glaciers exhibit a strong heterogeneity. Generally, the glacier thickness increases from the Westerly-dominated zone Pamir–Karakoram ($-0.10 \pm 0.10 \text{ m yr}^{-1}$) to the two edges, that is, Tien Shan ($-0.50 \pm 0.10 \text{ m yr}^{-1}$) in the northeast and Himalaya ($-0.59 \pm 0.10 \text{ m yr}^{-1}$) and Nyaingentanglha in the southeast.

282



283

284

Figure 2. Glacier thickness changes in High Mountain Asia (2003–2019). Map of the average glacier thickness change on a $1^\circ \times 1^\circ$ grid covering rectangular averaging cells of $2^\circ \times 2^\circ$. The change trend was obtained by the linear regression of data from the autumn campaign of ICESat-1,2. The background is ESRI imagery World from ArcGIS Online.

288

289

4. Discussion

290

4.1 Comparison with other recent studies

291

292

Based on efforts regarding the estimation of HMA glaciers, the spatial variability of the glacier changes could be well established. The results of several studies indicated the fastest melting for the Nyaingentanglha glacier, fewer changes in Karakoram, and positive changes in West Kunlun (Kääb *et al.*, 2015; Brun *et al.*, 2017; Shean *et al.*, 2020). However, the change trend in several subregions and whole HMA remains controversial.

297

1) Comparison with GRACE/GRACE-FO-based studies

298

299

Overall, the mass budget determined for the HMA in this study, that is, approximately -28 Gt yr^{-1} , based on ICESat-1,2 is similar to -29 Gt yr^{-1} reported in

300

301 recent work based on GRACE/GRACE-FO (Ciraci *et al.*, 2020). Actually, the
302 estimate of Ciraci *et al.* (2020) includes other hydrological signals, such as lake water
303 in the ITP. They report $+2 \text{ Gt yr}^{-1}$ compared with -4 Gt yr^{-1} determined based on
304 ICESat-1,2 in this study. Excluding the ITP glacier, we obtained $-23 \pm 3 \text{ Gt yr}^{-1}$ based
305 on GRACE and $-24 \pm 6 \text{ Gt yr}^{-1}$ based on ICESat-1,2 compared with $-32 \pm 6 \text{ Gt yr}^{-1}$
306 reported in Ciraci *et al.* (2020). Note that the corrected terms (GIA, hydrological
307 leakage) in Ciraci *et al.* (2020) are relatively large (approximately -18 Gt yr^{-1}) and
308 thus greatly affect the final result, accounting for $\geq 60\%$ of the total mass budget. Only
309 GRACE result is $-10/-18 \text{ Gt yr}^{-1}$ in the HMA/HMA (excluding the ITP) in Ciraci *et al.*
310 (2020). Our GRACE or GRACE-GLDAS-based mass change is in better agreement
311 with ICESat-based estimates than the value after removing the corrected terms such
312 as GIA. Thus, one must be cautious when using the corrected terms based on the
313 tectonic model.

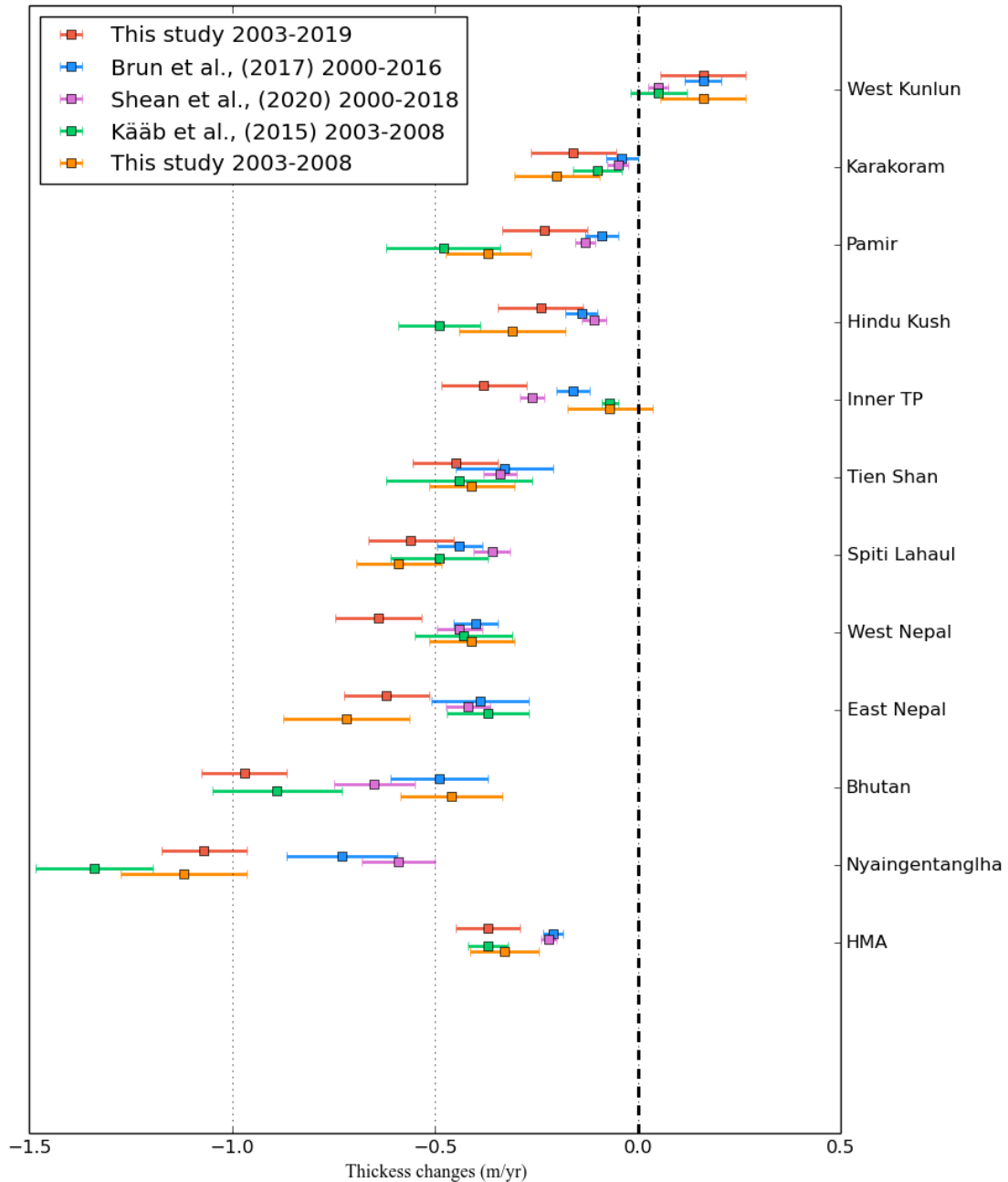
314 1) Comparison with satellite stereo imagery-based studies

315 Our result ($-28 \pm 6 \text{ Gt yr}^{-1}$) for the period 2003–2019 is more negative than that
316 reported for the periods 2000–2016 ($-16 \pm 4 \text{ Gt yr}^{-1}$; Brun *et al.*, 2017) and 2000–2018
317 ($-19 \pm 3 \text{ Gt yr}^{-1}$; Shean *et al.*, 2020). To analyze the divergence and directly compare
318 it with satellite stereo imagery, we followed the division of Brun *et al.* (2017) and
319 Kääb *et al.* (2015). The glacier thickness change was determined to avoid uncertainty
320 caused by the volume-to-mass conversion. Compared with Brun *et al.* (2017), the
321 glacier thickness changes in six of the eleven regions are within two standard
322 deviations (± 2 sigma), as shown in Fig. 3 and Table S1. The remaining five regions
323 are West Nepal, East Nepal, Bhutan, Nyaingentanglha, and the ITP. The largest
324 divergence was observed in Bhutan with a 2400 km^2 glacier area. The number of
325 available data might be affected by a small subregion. Compared with recent stereo
326 imagery-based work (Shean *et al.*, 2020), the period 2000–2018 is close to that used
327 in our studies. Nine of eleven regions are within two standard deviations. The increase
328 in the percentage is due to improved performances in the ITP (significant
329 improvement), West Nepal, and East Nepal. This difference is partly due to the
330 different study periods. In general, ICESat-1,2-based results are more negative than
331 satellite stereo imagery-based results, especially in areas with rapidly thickening
332 glaciers such as the southeastern Himalaya (Nepal and Bhutan) and Nyaingentanglha.

333 2) Comparison with ICESat-1-based studies

334 Six out of the eleven subregions are within two standard deviations. Considering
335 the short period (2003–2008) of previous ICESat-1-based studies, the difference
336 might be due to glacier changes in the recent decade. We present the glacier thickness
337 changes based on ICESat-1 for comparison (Fig. 3 and Table S1). Our results are in
338 good agreement with those of previous studies in nine of eleven regions. The two
339 divergent regions are the Bhutan and East Nepal (called Everest in Kaab *et al.*, 2015)
340 glaciers. Based on our work, these two subregions are relatively small, that is, ~ 2400
341 and 4900 km^2 . These values contrast those reported by Kaab *et al.* (2015) are 3500
342 and 8500 km^2 , respectively. The large difference in the division and glacier inventory

343 might be the reason for the different estimates. If we treat the two subregions as one
 344 subregion, the divergence improves by approximately -0.63 m yr^{-1} in this study and
 345 -0.52 m yr^{-1} in Kaab et al. (2015). In total, ICESat-1- and ICESat-1,2-based results
 346 demonstrate a strong ablation in Nyaingentanglha/Bhutan, that is, thickness changes
 347 of $\sim 1 \text{ m yr}^{-1}$, which are more negative than the results obtained from satellite stereo
 348 image-based studies.



349
 350 Figure 3. The comparison of glacier thickness changes from this study and previous
 351 results. The Errors are given at the 1σ level. Kääb et al., (2015) did not provide the
 352 glacier trend in inner TP, Tien Shan, but Brun et al., (2017) provide missing value by
 353 use same method of Kääb et al., (2015).
 354

355 4.2 Error analysis and choice of hyperparameters

356 The uncertainty calculation of DH (error bar in Fig. 1) follows Wang et al.
357 (2017b):

$$\sigma_{DH} = \sqrt{\sigma_{std}^2 + \sigma_{dh}^2}, \quad (1)$$

358 where σ_{std}^2 is the standard deviation of the parameters for the different widths of
359 elevation bins ranging from 100 to 600 m spaced at 100 m intervals; σ_{dh}^2 is the error
360 of dh due to vertical SRTM (7–12 m), ICESat errors, and radar penetration; and σ_{dh}^2
361 was set to 20 m based on the footprint in this study.

362 The total uncertainty of the glacier mass budget consists of three parts: 1)
363 *autumn DH* trend, 2) glacier area uncertainty, and 3) uncertainty in the density
364 assumption. We considered an uncertainty of 10% for the glacier area and density.
365 The autumn trend was estimated using Eq. (2):

$$\sigma_{DH/dt} = \sqrt{\sigma_{fit}^2 + \sigma_{spat}^2 + \sigma_{temp}^2 + \sigma_{bais}^2}, \quad (2)$$

366 where σ_{dh}^2 is the linear fitting error, σ_{spat}^2 and σ_{temp}^2 are the irregular spatial and
367 temporal ICESat sampling errors, respectively; and σ_{bais}^2 is the unknown systematic
368 uncertainty considering intercomparison biases and crustal uplift. In this study, σ_{spat}^2 ,
369 σ_{temp}^2 , and σ_{bais}^2 were set to 0.06, similar to previous studies (*Gardner et al.*, 2013;
370 *Farinotti et al.*, 2015).

371 1) Spatial glacier coverage

372 The ICESat measurement of the changes in the glacier thickness only covers the
373 region with footprints. Therefore, extrapolation to the whole glacier area is necessary.
374 In this study, the extrapolation was carried out as follows: 1) The mean altitude (h_g)
375 and standard deviation (h_{std}) of the glaciers in each subregion were calculated. The
376 results of ~95% of the glaciers with altitudes ranging from $h_g - 2h_{std}$ to $h_g + 2h_{std}$ were
377 determined in their corresponding elevation bin (see glacier altitude histogram Fig.
378 S2). The extrapolation was based on the assumption that glaciers in the same
379 elevation range exhibit the same changes; and 2) the remaining ~5% of glaciers were
380 added to the calculation of the mass budget and the results of 95% of the glaciers
381 were used.

382 2) Linear regression and ICESat observation campaign

383 Due to strong snowfall or snowpack in winter, the winter campaign of ICESat
384 was not used for the linear regression in most previous ICESat-based studies of HMA
385 glaciers. In this study, all glacier change trends (Figs 1 and 2, Table S1) are based on
386 the linear regression of the ICESat autumn campaign. Note that the result of the
387 ICESat winter campaign is presented in Fig. 1; however, it was not used for the
388 regression model. Due to the long temporal span after the combination of ICESat-1
389 and 2, the linear regressions without or with the winter campaign insignificantly differ.
390 In addition, to maintain consistency with the ICESat-1 observation, we used the same
391 time window to obtain the autumn and winter observation of ICESat-2. Although the

392 downsampling of ICESat-2 will lead to the loss of data, it helps to reduce the bias in
393 the mass budget evaluation and keep consistency with ICESat-1.

394

395

396 **5. Conclusions**

397 This study demonstrates the first results on recent glacier surface changes in the
398 HMA region based on ICESat-2. The total mass balances and changes in the thickness
399 of the HMA glacier from 2003–2019 (~17 years) were determined by combining
400 ICESat-1 and 2. We used GRACE data to fill the data gap of ICESat-1,2 from 2010 to
401 2017 and provided a continuous time series of the glacier mass change in the HMA
402 and its four subregions. The comparison of ICESat-1,2 and GRACE/GRACE-FO
403 shows that these data are in excellent agreement at the total and regional scales ($r =$
404 0.9 , $p < 0.0001$). This consistency between the two independent approaches indicates
405 the high reliability of HMA glacier mass change data and validates the calculations
406 based on two sets of satellite observations. Based on this study, that is, the use of
407 ICESat-1,2 data from March 2003 to November 2019, the total mass budget of the
408 HMA glaciers is $-28 \pm 6 \text{ Gt yr}^{-1}$. On the periphery of the Tibetan Plateau, including
409 Tien Shan, Pamir–Karakoram, Himalaya, and Nyaingentanglha, the mass budget of
410 the glaciers in the period 2003 to 2019/2020 is $-24 \pm 5 \text{ Gt yr}^{-1}$ based on ICESat, $-23 \pm$
411 3 Gt yr^{-1} based on GRACE, and $-28 \pm 3 \text{ Gt}$ based on GRACE with GIA-corrected
412 terms. Based on the spatial heterogeneity of the glacier change rates, the most
413 negative value is observed in Nyaingentanglha ($-1.07 \pm 0.10 \text{ m yr}^{-1}$), followed by the
414 Himalayas ($-0.58 \pm 0.10 \text{ m yr}^{-1}$), Tien Shan ($-0.45 \pm 0.10 \text{ m yr}^{-1}$), and Pamir–
415 Karakoram ($-0.10 \pm 0.10 \text{ m yr}^{-1}$). The West Kunlun glaciers slightly increased by
416 approximately $+0.16 \pm 0.10 \text{ m yr}^{-1}$. Based on ICESat2 and GRACE-FO, the HMA
417 glacier changes can be continuously monitored.

418

419 **6. Acknowledgements**

420 We are grateful for the financial support from the Natural Science Foundation of
421 China (41774088, 41974093, 41331066, and 41474059), Key Research Program of
422 Frontier Sciences of the Chinese Academy of Sciences (QYZDY-SSW-SYS003), and
423 fellowships of the China Postdoctoral Science Foundation (2020M670424 and
424 2020T130641). The data used in this study are publicly open, and their sources are
425 indicated in the “Data and Method” section. ICESat-1,2 data are provided by National
426 Snow & Ice Data Center and available at the website (<https://nsidc.org/data/icesat> and
427 <https://nsidc.org/data/icesat-2>). GRACE and GRACE-FO data are provided by the
428 University of Texas and available at the website (<http://www2.csr.utexas.edu/grace/>).
429 The GLDAS-2.1 data are available at the website
430 (https://disc.gsfc.nasa.gov/datasets/GLDAS_NOAH025_3H_2.1/summary).

431

432 REFERENCES

- 433 Argus, D. F., W. R. Peltier, R. Drummond, and A. W. Moore (2014), The Antarctica
434 component of postglacial rebound model ICE-6G_C (VM5a) based on GPS
435 positioning, exposure age dating of ice thicknesses, and relative sea level
436 histories, *Geophysical Journal International*, 198(1), 537-563,
437 doi:10.1093/gji/ggu140.
- 438 Azam, M. F., P. Wagnon, E. Berthier, C. Vincent, K. Fujita, and J. S. Kargel (2018),
439 Review of the status and mass changes of Himalayan-Karakoram glaciers,
440 *Journal of Glaciology*, 64(243), 61-74, doi:10.1017/jog.2017.86.
- 441 Beaudoin H, Rodell M. GLDAS Noah Land Surface Model L4 3 hourly 0.25× 0.25
442 degree V2. 1[J]. Goddard Earth Sciences Data and Information Services
443 Center (GES DISC): Greenbelt, MD, USA, 2016.
- 444 Bettadpur, S. (2012). UTCSR level - 2 processing standards document, technical
445 report GRACE. Austin, Texas: Center for Space Research, University of
446 Texas.
- 447 Bolch, T., A. V. Kulkarni, A. Kaab, C. Huggel, F. Paul, J. G. Cogley, H. Frey, J. S.
448 Kargel, K. Fujita, and M. Scheel (2012), The State and Fate of Himalayan
449 Glaciers, *Science*, 336(6079), 310-314.
- 450 Brun, F., E. Berthier, P. Wagnon, A. Kääh, and D. Treichler (2017), A spatially
451 resolved estimate of High Mountain Asia glacier mass balances from 2000 to
452 2016, *Nature Geoscience*, 10(9), 668-673, doi:10.1038/ngeo2999.
- 453 Brunt, K. M., T. A. Neumann, and B. E. Smith (2019), Assessment of ICESat-2 Ice
454 Sheet Surface Heights, Based on Comparisons Over the Interior of the
455 Antarctic Ice Sheet, *Geophysical Research Letters*, 46(22), 13072-13078,
456 doi:10.1029/2019gl084886.
- 457 Cheng, M., J. Ries, and B. Tapley (2013), Geocenter variations from analysis of SLR
458 data, in *Reference Frames for Applications in Geosciences*, edited, pp. 19-25,
459 Springer.
- 460 Ciraci, E., I. Velicogna, and S. Swenson (2020), Continuity of the Mass Loss of the
461 World's Glaciers and Ice Caps From the GRACE and GRACE Follow-On
462 Missions, *Geophysical Research Letters*, 47(9), e2019GL086926,
463 doi:10.1029/2019gl086926.
- 464 Farinotti, D., L. Longuevergne, G. Moholdt, D. Duethmann, T. Mölg, T. Bolch, S.
465 Vorogushyn, and A. Güntner (2015), Substantial glacier mass loss in the
466 Tien Shan over the past 50 years, *Nature Geoscience*.
- 467 Farr, T. G., et al. (2007), The Shuttle Radar Topography Mission, *Reviews of*
468 *Geophysics*, 45(2), RG2004, doi:10.1029/2005rg000183.
- 469 Gardelle, J., E. Berthier, and Y. Arnaud (2012), Slight mass gain of Karakoram
470 glaciers in the early twenty-first century, *Nature Geoscience*, 5(5), 322-325,
471 doi:10.1038/ngeo1450.

472 Gardelle, J., E. Berthier, Y. Arnaud, and A. Kaab (2013), Region-wide glacier mass
473 balances over the Pamir-Karakoram-Himalaya during 1999-2011 (vol 7, pg
474 1263, 2013), *The Cryosphere*, 7(6), 1885-1886, doi:10.5194/tc-7-1885-2013.

475 Gardner, A. S., et al. (2013), A Reconciled Estimate of Glacier Contributions to Sea
476 Level Rise: 2003 to 2009, *Science*, 340(6134), 852-857,
477 doi:10.1126/science.1234532.

478 Huss, M. (2013), Density assumptions for converting geodetic glacier volume change
479 to mass change, *The Cryosphere*, 7(3), 877-887.

480 Immerzeel, W. W., and M. F. P. Bierkens (2012), Asia's water balance, *Nature*
481 *Geosci*, 5(12), 841-842.

482 Immerzeel, W. W., et al. (2020), Importance and vulnerability of the world's water
483 towers, *Nature*, 577(7790), 364-369, doi:10.1038/s41586-019-1822-y.

484 Jacob, T., J. Wahr, W. T. Pfeffer, and S. Swenson (2012), Recent contributions of
485 glaciers and ice caps to sea level rise, *Nature*, 482(7386), 514-518,
486 doi:[http://www.nature.com/nature/journal/v482/n7386/abs/nature10847.html](http://www.nature.com/nature/journal/v482/n7386/abs/nature10847.html#supplementary-information)
487 [#supplementary-information](http://www.nature.com/nature/journal/v482/n7386/abs/nature10847.html#supplementary-information).

488 Kääh, A., E. Berthier, C. Nuth, J. Gardelle, and Y. Arnaud (2012), Contrasting
489 patterns of early twenty-first-century glacier mass change in the Himalayas,
490 *Nature*, 488(7412), 495-498, doi:10.1038/nature11324.

491 Kwok, R., G. Cunningham, T. Markus, D. Hancock, J. H. Morison, S. P. Palm, S. L.
492 Farrell, A. Ivanoff, J. Wimert, and the ICESat-2 Science Team. 2020.
493 ATLAS/ICESat-2 L3A Sea Ice Height, Version 3. [Indicate subset used].
494 Boulder, Colorado USA. NASA National Snow and Ice Data Center
495 Distributed Active Archive Center. doi:
496 <https://doi.org/10.5067/ATLAS/ATL07.003>. [Date Accessed].

497 Markus, T., Neumann, T., Martino, A., Abdalati, W., Brunt, K., Csatho, B., Farrell, S.,
498 Fricker, H., Gardner, A., Harding, D., Jasinski, M., Kwok, R., Magruder, L.,
499 Lubin, B., Luthcke, S., Morison, J., Nelson, R., Neuenschwander, A., Palm, S.,
500 Popescu, S., Shum, C., Schutz, B., Smith, B., Yang, Y., & Zwally, J. (2017).
501 The Ice, Cloud, and land Elevation Satellite - 2 (ICESat - 2): Science
502 requirements, concept, and implementation. *Remote Sensing of Environment*,
503 190, 260–273. <https://doi.org/10.1016/j.rse.2016.12.029>

504 Matsuo, K., and K. Heki (2010), Time-variable ice loss in Asian high mountains from
505 satellite gravimetry, *Earth and Planetary Science Letters*, 290(1–2), 30-36,
506 doi:<http://dx.doi.org/10.1016/j.epsl.2009.11.053>.

507 Neckel, N., J. Kropáček, T. Bolch, and V. Hochschild (2014), Glacier mass changes
508 on the Tibetan Plateau 2003–2009 derived from ICESat laser altimetry
509 measurements, *Environmental research letters*, 9(1), 014009.

510 Neumann, T. A., Brenner, A. C., Hancock, D. W., Harbeck, K., Luthcke, S., Robbins,
511 J., Saba, J., & Gibbons, A. (2018). Ice, Cloud, and Land Elevation Satellite-2
512 project algorithm theoretical basis document for global geolocated photons
513 (ATL03). <https://icesat-2.gsfc.nasa.gov/science/data-products>.

514 Neumann, T. A., Martino, A. J., Markus, T., Bae, S., Bock, M. R., Brenner, A. C.,
515 Brunt, K. M., Cavanaugh, J., Fernandes, S. T., Hancock, D. W., Harbeck, K.,
516 Lee, J., Kurtz, N. T., Luers, P. J., Luthcke, S. B., Magruder, L., Pennington, T.
517 A., Ramos - Izquierdo, L., Rebold, T., Skoog, J., & Thomas, T. C. (2019).
518 The Ice, Cloud, and Land Elevation Satellite - 2 Mission: A global geolocated
519 photon product. *Remote Sensing of Environment*, 233, 111325.
520 <https://doi.org/10.1016/j.rse.2019.111325>

521 Peltier, W. R., D. F. Argus, and R. Drummond (2015), Space geodesy constrains ice
522 age terminal deglaciation: The global ICE-6G_C (VM5a) model, *Journal of*
523 *Geophysical Research: Solid Earth*, 120(1), 450-487,
524 [doi:10.1002/2014jb011176](https://doi.org/10.1002/2014jb011176).

525 Pfeffer, W. T., A. Arendt, A. Bliss, T. Bolch, J. G. Cogley, A. S. Gardner, J. O.
526 Hagen, R. Hock, G. Kaser, and C. Kienholz (2014), The Randolph Glacier
527 Inventory : a globally complete inventory of glaciers, *Journal of Glaciology*,
528 60(221), 537-552.

529 Pritchard, H. D. (2019), Asia's shrinking glaciers protect large populations from
530 drought stress, *Nature*, 569(7758), 649-654,
531 [doi:10.1038/s41586-019-1240-1](https://doi.org/10.1038/s41586-019-1240-1).

532 RGI Consortium (2017). Randolph Glacier Inventory – A Dataset of Global Glacier
533 Outlines: Version 6.0: Technical Report, Global Land Ice Measurements from
534 Space, Colorado, USA. Digital Media. DOI:
535 <https://doi.org/10.7265/N5-RGI-60>

536 Schrama, E. J. O., B. Wouters, and R. Rietbroek (2014), A mascon approach to assess
537 ice sheet and glacier mass balances and their uncertainties from GRACE
538 data, *Journal of Geophysical Research: Solid Earth*, 119(7), 6048-6066,
539 [doi:10.1002/2013jb010923](https://doi.org/10.1002/2013jb010923).

540 Shean, D. E., S. Bhushan, P. Montesano, D. R. Rounce, A. Arendt, and B. Osmanoglu
541 (2020), A Systematic, Regional Assessment of High Mountain Asia Glacier
542 Mass Balance, *Frontiers in Earth Science*, 7(363),
543 [doi:10.3389/feart.2019.00363](https://doi.org/10.3389/feart.2019.00363).

544 Swenson, S., D. Chambers, and J. Wahr (2008), Estimating geocenter variations from
545 a combination of GRACE and ocean model output, *Journal of Geophysical*
546 *Research: Solid Earth*, 113(B8), [doi:10.1029/2007jb005338](https://doi.org/10.1029/2007jb005338).

547 Treichler, D., A. Käab, N. Salzmann, and C. Y. Xu (2019), Recent glacier and lake
548 changes in High Mountain Asia and their relation to precipitation changes,
549 *The Cryosphere*, 13(11), 2977-3005, [doi:10.5194/tc-13-2977-2019](https://doi.org/10.5194/tc-13-2977-2019).

550 Treichler, D., C. Nuth, and E. Berthier (2015), Brief Communication: Contending
551 estimates of 2003--2008 glacier mass balance over the
552 Pamir-Karakoram-Himalaya, *The Cryosphere*, 9, 557.

553 Velicogna, I. (2009), Increasing rates of ice mass loss from the Greenland and
554 Antarctic ice sheets revealed by GRACE, *Geophysical Research Letters*,
555 36(19).

556 Wang, Q., S. Yi, L. Chang, and W. Sun (2017a), Large-Scale Seasonal Changes in
557 Glacier Thickness Across High Mountain Asia, *Geophysical Research*
558 *Letters*, 44(20), 10,427-410,435, doi:10.1002/2017gl075300.

559 Wang, Q., S. Yi, and W. Sun (2016), The changing pattern of lake and its contribution
560 to increased mass in the Tibetan Plateau derived from GRACE and ICESat
561 data, *Geophysical Journal International*, 207(1), 528-541,
562 doi:10.1093/gji/ggw293.

563 Wang, Q., S. Yi, and W. Sun (2017b), Precipitation-driven glacier changes in the
564 Pamir and Hindu Kush mountains, *Geophysical Research Letters*, 44(6),
565 2817-2824, doi:10.1002/2017gl072646.

566 Wang, Q., S. Yi, and W. Sun (2018), Consistent interannual changes in glacier mass
567 balance and their relationship with climate variation on the periphery of the
568 Tibetan Plateau, *Geophysical Journal International*, 214(1), 573-582,
569 doi:10.1093/gji/ggy164.

570 Wouters, B., A. S. Gardner, and G. Moholdt (2019), Global glacier mass loss during
571 the GRACE satellite mission (2002-2016), *Frontiers in Earth Science*, 7,
572 doi:Urn:Nbn:Nl:Ui:10-1874-385100.

573 Yao, T., et al. (2012), Different glacier status with atmospheric circulations in Tibetan
574 Plateau and surroundings, *Nature Clim. Change*, 2(9), 663-667,
575 doi:[http://www.nature.com/nclimate/journal/v2/n9/abs/nclimate1580.html#su](http://www.nature.com/nclimate/journal/v2/n9/abs/nclimate1580.html#supplementary-information)
576 [pplementary-information](http://www.nature.com/nclimate/journal/v2/n9/abs/nclimate1580.html#supplementary-information).

577 Yao, T., et al. (2019), Recent Third Pole's Rapid Warming Accompanies Cryospheric
578 Melt and Water Cycle Intensification and Interactions between Monsoon and
579 Environment: Multidisciplinary Approach with Observations, Modeling, and
580 Analysis, *Bulletin of the American Meteorological Society*, 100(3), 423-444,
581 doi:10.1175/bams-d-17-0057.1.

582 Yi, S., and W. Sun (2014), Evaluation of glacier changes in high-mountain Asia based
583 on 10 year GRACE RL05 models, *Journal of Geophysical Research: Solid*
584 *Earth*, 119(3), 2013JB010860, doi:10.1002/2013jb010860.

585 Yi, S., Q. Wang, L. Chang, and W. Sun (2016), Changes in Mountain Glaciers, Lake
586 Levels, and Snow Coverage in the Tianshan Monitored by GRACE, ICESat,
587 Altimetry, and MODIS, *Remote Sensing*, 8(10), 798.

588 Zhang, G., T. Yao, H. Xie, S. Kang, and Y. Lei (2013), Increased mass over the
589 Tibetan Plateau: from lakes or glaciers?, *Geophysical Research Letters*,
590 40(10), 2125-2130.

591